Wave-equation migration of common-receiver gathers for AVO analysis

GUY PURNELL, DWIGHT SUKUP, and JOE HIGGINBOTHAM, ChevronTexaco, Houston, Texas, U.S.

During the 1980s and 1990s, we developed a number of recursive wave-equation algorithms for prestack depth migration in the shot domain. Much of that work was driven by development of the vertical-cable recording technique. However, we applied the algorithms to image a variety of 2D and 3D land and marine surveys. Virtually all of those projects were oriented toward obtaining better structural images and without concern for preserving relative amplitude information.

Increasing interest in prestack amplitude analysis of migrated data led us to revisit that decision and to evaluate the possibility of analyzing AVO (or AVA) within image gathers. Developers of other wave-equation-based algorithms have presented similar evaluations and have achieved useful results. However, our production algorithms are sufficiently different that the applicability of their results to our project work is not clear. Consequently, we decided to conduct our own study, starting with a modeling-based approach—rather than a theoretical one—to analyze application of one of our 3D shot-record depth migration algorithms to synthetic and real data. The immediate value of this would be as a measure of the "amplitude-friendliness" of an existing production algorithm under specific conditions. Beyond that, it would help us gauge the potential value of allocating additional theoretical and/or development work to enhance its usefulness as a tool for amplitude studies in projects involving wave-equation shot-record migration.

The real data set we selected for testing is an OBC survey recorded by Texaco in 1997 at Teal South Field (Eugene Island Block 354) in the Gulf of Mexico. This survey was used 24 4C receiver groups fixed in a sparse pattern on the seafloor, about 82 m deep (Figure 1). The source was a small air-gun array towed at a depth of 3 m and was deployed at locations on a finer (nominally 25 × 25 m) grid covering a 3 × 3 km area. A rather pronounced footprint effect is associated with the sparse receiver grid. Although it diminishes with depth, it still poses a challenge to amplitude analysis.

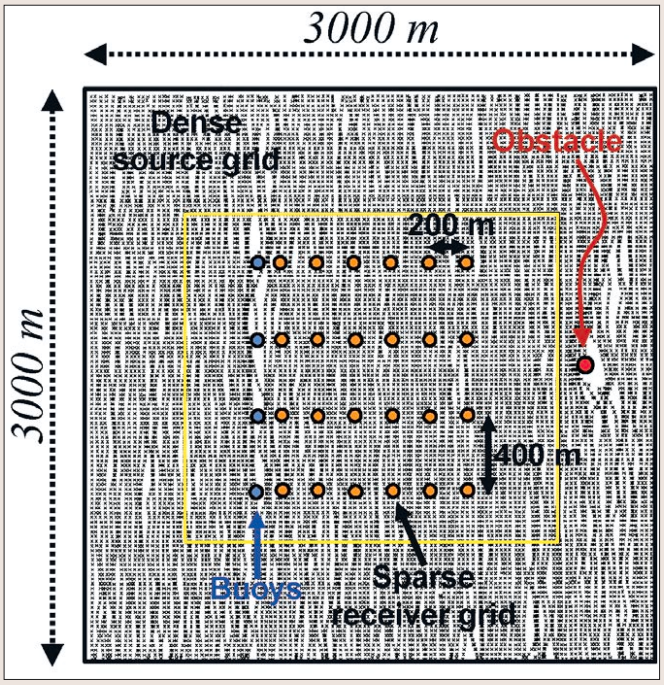

Figure 1. Acquisition geometry for the 1997 OBC survey. Twenty-four fixed 4C receivers recorded the wavfields produced by ~ 14 400 shots distributed across a 3×3-km area.

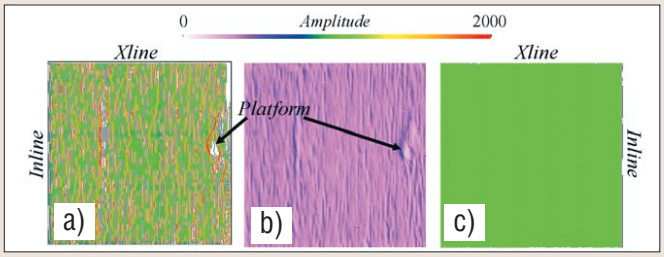

Figure 2. Spatial distribution of amplitudes after regularizing a synthetic common-receiver gather. The input gather contained a single constant-amplitude reflection from a horizontal interface, as would be recorded by a receiver centered in a source grid identical to that in Figure 1. (a) Two-pass f-x interpolation followed by binning. (b) 3D τ-p,q regridding. (c) Polynomial x-y regridding.

Strategy for data processing and analysis. Our plan was to reprocess the hydrophone component using a conventional AVO-preprocessing sequence, apply 3D prestack migration, and analyze the AVO in image gathers. For the analysis, we would use a simple technique to calculate incidence angles, based on simplifying assumptions valid for the test area.

The geometry of the survey is akin to that of a vertical-cable survey (e.g., Krail, 1994) reduced to having only one receiver level. As such, it can be imaged in a similar way. The key component of our processing methodology for vertical-cable surveys is 3D wave-equation migration of common-receiver gathers (CRGs). In order to carry this out, we invoke reciprocity to swap the roles of source and receiver, then apply a shot-record migration to each CRG. The entire survey consists of only 24 CRGs, so 3D shot-record migration is much more efficient than it would be for conventional marine-streamer surveys.

Because the detectors are on the seafloor, upgoing waves (e.g., primary reflections) and downgoing waves (e.g., receiver-ghost arrivals associated with primaries reflected at the sea surface) appear as discrete events that can be imaged separately. A discussion of that is outside the scope of this paper; however, the processing conformed to our (then) normal vertical-cable/OBC practice and included no premigration processing to attenuate the receiver ghost. All prestack-migration examples in this paper result from migration applied to properly image the upgoing waves. Consequently, the images contain some spurious events associated with unattenuated downgoing waves.

After the notional source-receiver swap, PSPI (extrapolation using one-way phase-shift-plus-interpolation) was used to iteratively downward continue the "upgoing" wavefield incident at the "receivers." For the "downgoing" wavefield, we had the option to use PSPI to model the wavefield radiating from a synthetic source (which, in reality, is at the receiver location). As an alternative, we predicted first-arrival traveltimes from a synthetic source using the eikonal equation. At each downward-continuation step, a slab of the output image volume is constructed by extracting the portion of the upgo-

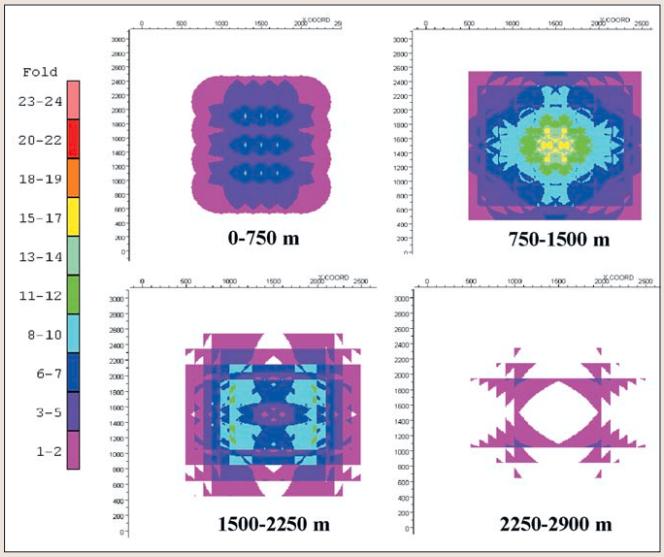

Figure 3. *CMP fold for different offset ranges.*

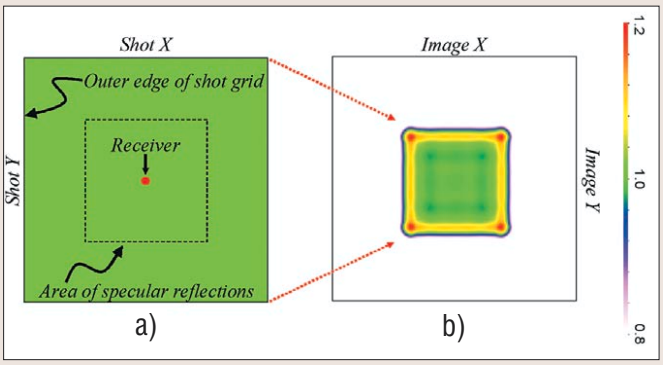

Figure 4. *Spatial distribution of amplitudes before and after migrating a synthetic common-receiver gather containing a single constant-amplitude reflection from a horizontal interface. Before migration (a), the event amplitude is uniform. After migration (b), the area of specular reflection is imaged with nearly uniform amplitudes, except near its perimeter. The edge effect is associated with the finite extent of the source grid.*

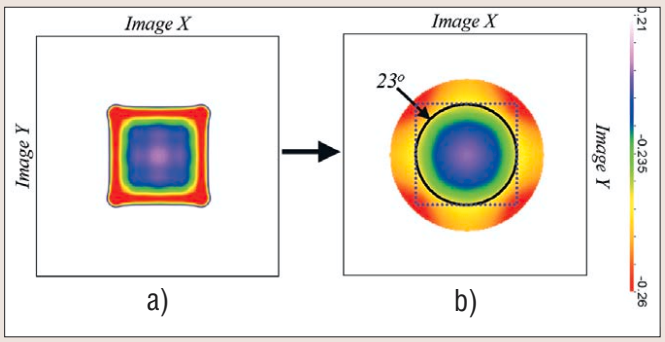

Figure 5. *Spatial distribution of amplitudes after migrating a synthetic common-receiver gather containing a single nonconstant-amplitude reflection from a horizontal interface. The reflection corresponds to a class-III AVO anomaly. (a) Image output by the migration exhibits the combined effects of limited source extent and class-III AVO. (b) After model-based compensation for the source-grid footprint, the true AVO behavior is more readily apparent. 23° is the maximum incidence angle for which a specular reflection is imaged at all source-receiver azimuths.*

ing wavefield that coincides with the downgoing traveltime at that depth. Thus, the imaging condition applied here is not a "true reflection-coefficient" type, in which the ratio of the upgoing and downgoing wavefields is taken. Rather, the image amplitude is proportional to the amplitude of the reflected wave at the reflector. This condition is easier to imple-

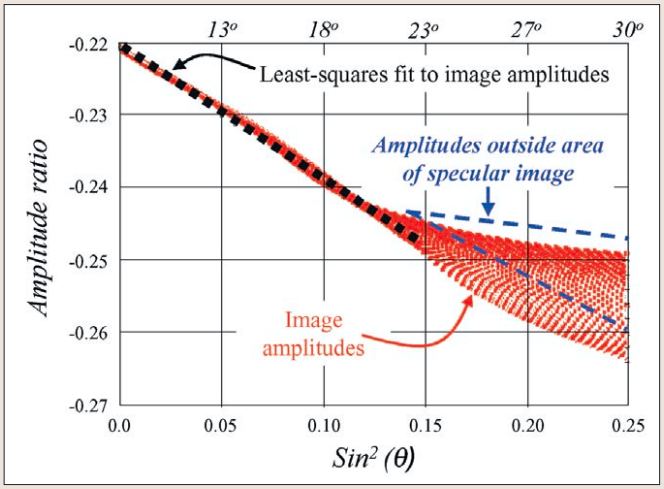

Figure 6. *Angular distribution of amplitudes (red dots) for the migrated reflection in Figure 5b. A least-squares fit (dashed black line) for angles less than 23° closely reproduces the behavior expected from the Zoeppritz equations. At higher angles, some image amplitudes come from within the area of specular imaging and are also useful.*

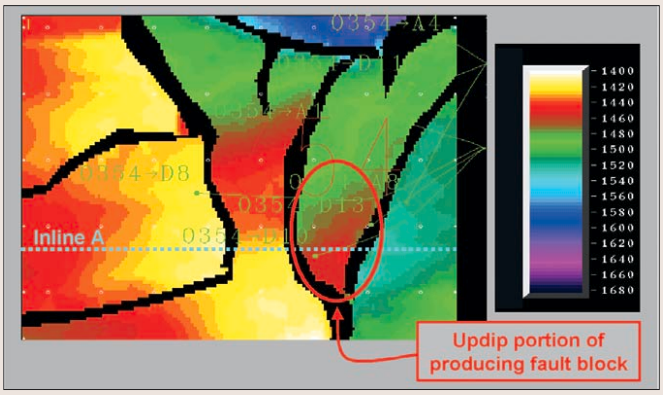

Figure 7. *Structure map (in two-way time) for top of the 4500-ft sand. High-GOR oil is produced from the updip portion of this sand in one fault block (red oval). An associated bright spot is evident on seismic lines (e.g., inline A) that traverse the updip portion of the reservoir.*

ment and may have value in situations where the overburden is not too complex (i.e., variable illumination of the reflector), such as at Teal South. Our idea was that a successful result here would encourage efforts to modify the algorithm to handle a more complex overburden.

Preliminary synthetic-data tests. Before putting our processing strategy into practice, we examined a few issues in greater detail.

Our migration algorithm requires that input CRGs consist of traces recorded from shots on a regular grid, rather than the actual grid (Figure 1), which is slightly irregular and has some larger gaps associated with surface obstacles. Consequently, we must regularize the gathers. Figure 2 demonstrates regularization results from three algorithms applied to a synthetic CRG containing a constant-amplitude event. The event simulates what a receiver beneath the center of the actual irregular source grid would record for reflections from a horizontal interface at depth. The reflector depth and velocity field above it correspond to Teal South examples shown in subsequent figures.

Regularization using tools applied in previous structural-imaging projects tended to introduce spurious amplitude variations (Figures 2a and 2b). If certain amplitude-balancing processes (e.g., AGC) were applied, such distortions might be masked and consequently overlooked. As an alternative, we

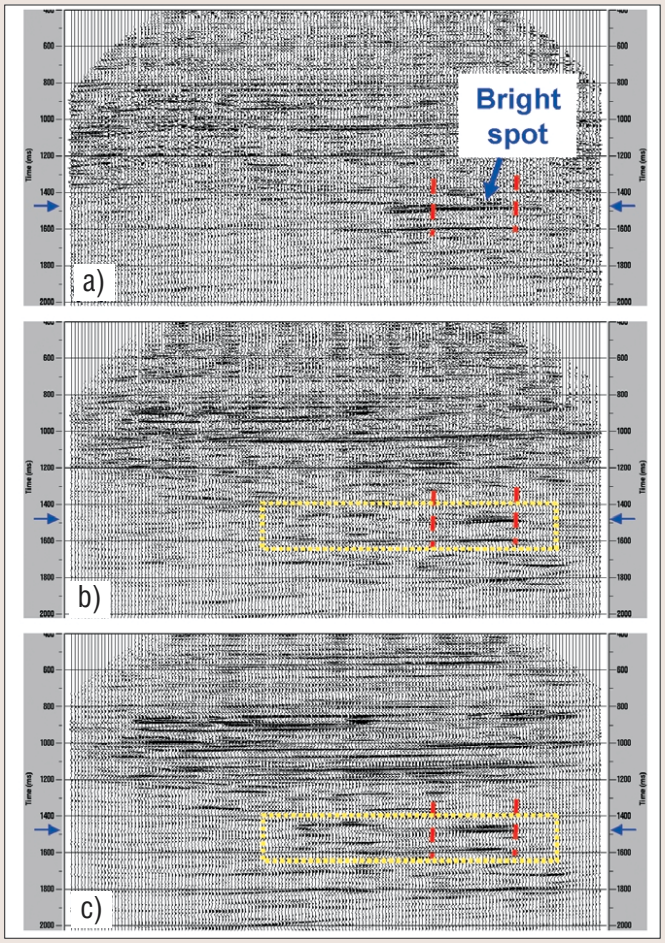

Figure 8. *Inline A after (a) CMP stack, (b) CMP stack + poststack time migration, and (c) prestack depth migration (converted to two-way vertical time).*

devised a regridding procedure based on local polynomial fitting to data that are irregularly located in both horizontal coordinates. This regularized the data with a very low level of distortion (Figure 2c).

The receiver grid, on the other hand, is so sparse that we chose not to attempt to regularize it or to simulate a denser grid. The distribution of azimuths and offsets in CMP bins, therefore, are highly variable spatially (e.g., Figure 3). Consequently, the receiver-grid footprint effect is much more serious than that associated with the source grid. However, it does not affect the image generated from migrating a single CRG; rather, it is manifested when the migrated CRGs are composited to form the final image volume.

One could decide to accept the receiver-grid footprint effect and deal with it in the amplitude analysis/interpretation phase. In that case, it is still useful to know how well the process of migrating individual CRGs preserves recorded AVO effects. Therefore, we decided to investigate the amplitude effects of our migration operator using a modeling approach.

Figure 4 shows the spatial distribution of amplitudes before and after migrating the synthetic common-receiver gather (with a constant-amplitude event) in Figure 2c. After migration, the amplitude behavior of the input data is preserved well, except near the edges of the imaged region. This appears to be a data-truncation effect associated with the finite source grid. It is undesirable, because it could introduce spurious AVO effects. One way to mitigate the practical consequences of the effect would be to use a larger source grid. A more economical way would be to compensate for the effect. We evaluated the latter approach using a simple prototype of a scheme designed to undo the modeled effect.

Migrating a synthetic CRG that contains a reflection that—instead of having constant amplitude—exhibits class-III AVO behavior yields the result in Figure 5a. In this example, the effects of data truncation and class-III AVO interfere con-

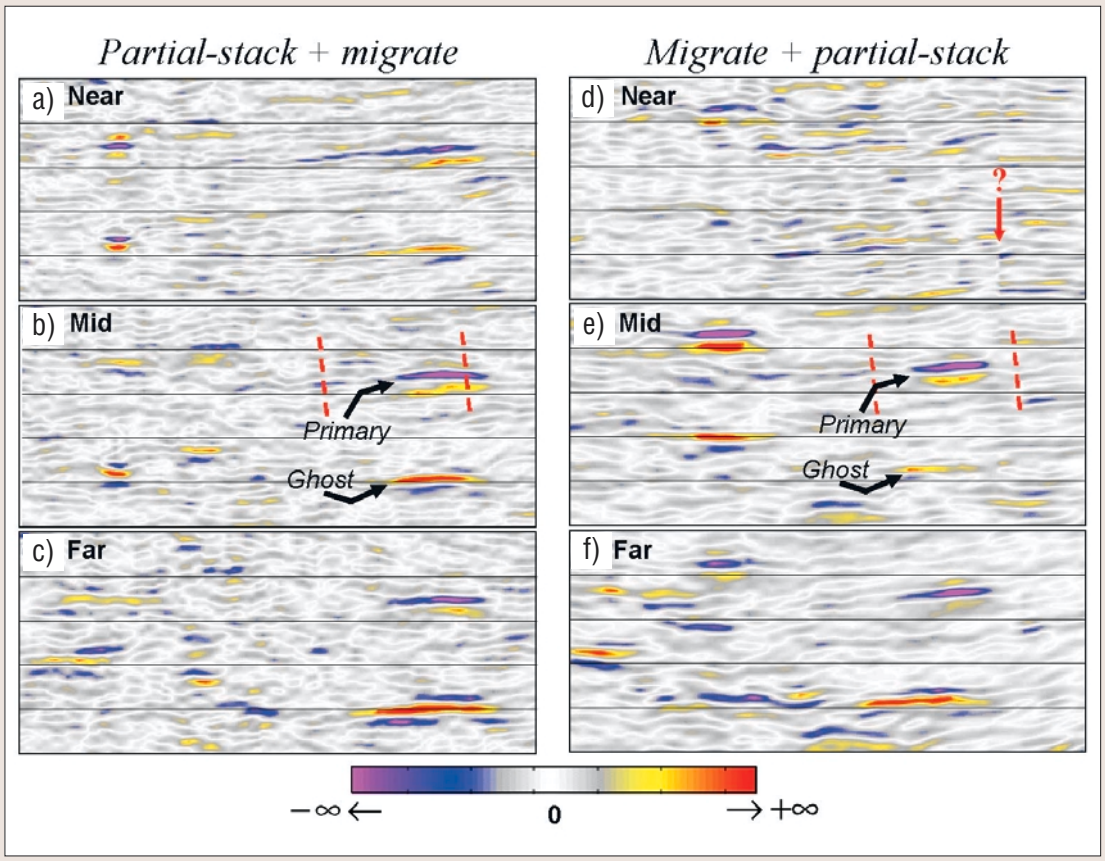

Figure 9. *Near-, mid-, and far-offset stacks for the region of inline A indicated by the yellow rectangles in Figure 8. (a-c) Poststack time migration of partial stacks. (d-f) Partial stacks after prestack depth migration (converted to two-way vertical time). In (d), the ? indicates a suspected acquisition footprint effect in the low-fold near-offset stack.*

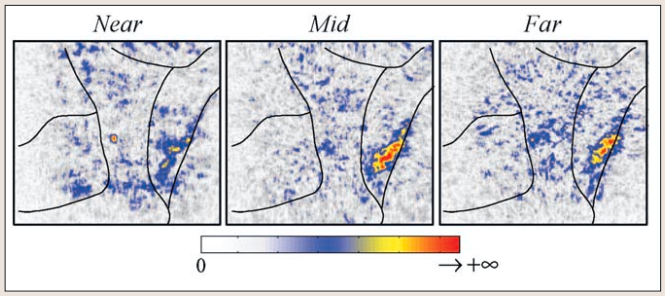

Figure 10. *Poststack time migrations of near-, mid-, and far-offset stacks (time slices at t=1476 ms through instantaneous amplitude volume).*

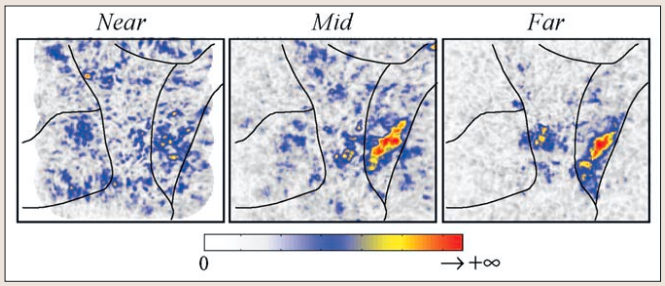

Figure 11. *Near-, mid-, and far-offset stacks of the data after prestack depth migration (time slices at t=1476 ms through instantaneous amplitude volume, after conversion to two-way vertical time).*

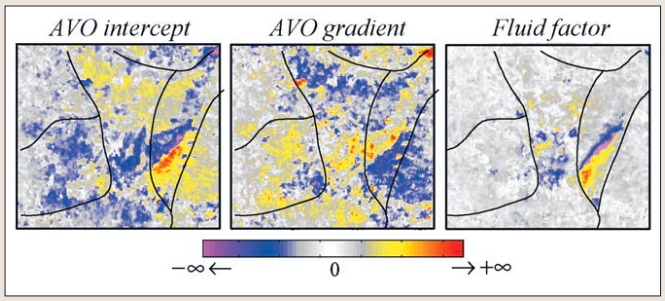

Figure 12. *AVO attributes calculated from linearized AVO inversion after prestack depth migration (time slices at t=1476 ms, after conversion to two-way vertical time).*

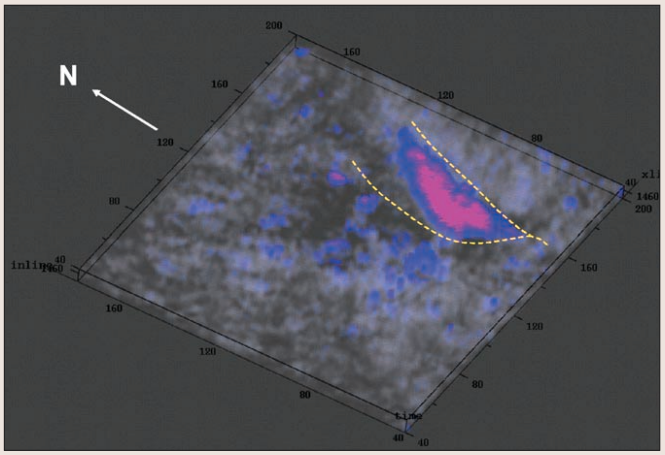

Figure 13. *Volume visualization of the envelope of the fluid factor, with small values rendered transparent. As expected from rock-physics modeling, large values tend to be confined to the updip portion of the producing fault block.*

structively. After applying the compensation prototype to the migrated CRG, the image amplitudes are more consistent with the true AVO behavior (Figures 5b and 6). The compensation was accomplished by weighting the image volume by a spatially varying scale factor, designed by modeling the edge effect at different depths.

The prototype compensation algorithm worked well on synthetic data. When applied to the real data, it had a relatively minor effect on the amplitude distributions. The largest effect was to accentuate footprint effects near the edges of the survey, so we decided to omit the compensation step from the final processing sequence.

Discussion. In our study, we focused on the "4500 ft" sand, a reservoir compartmentalized by faulting (Figure 7). High GOR oil is produced from that sand in the highlighted fault block.

As a first check on the data-processing results, we compared (Figure 8) a CMP stack to two image volumes: a poststack time migration and a prestack depth migration (the latter being a stack of image gathers after migration). In the unmigrated CMP stack, bright hydrocarbon-related events appear to extend across bounding faults that separate adjacent productive and unproductive fault blocks. Of the two migrated volumes, the prestack-migration image is somewhat better focused and has a cleaner appearance. Nevertheless, they are fairly consistent in their delineation of fault-block boundaries and hydrocarbon-related amplitude anomalies. Additional corroboration is provided by well control and 3D poststack migrations of earlier streamer data. It is apparent that for poststack amplitude analysis (e.g., bright-spot prospecting) here, poststack migration is adequate. However, for prestack study (e.g., AVO analysis), prestack migration is necessary if anomalies are to be interpreted at the correct locations.

Next, we examined near-, mid-, and far-offset stacks, and compared the results of migrating before or after stack (Figures 9-11). We found this approach to 3D amplitude analysis useful for identifying bright spots and AVO anomalies in their correct locations. However, interpretation of partial stacks is complicated by the acquisition footprint. This is particularly so for the near-offset stacks, for which the fold is lowest (Figure 3). This introduces ambiguity into the result of estimating the AVO gradient by subtracting far- and near-offset stacks.

We hypothesized that AVO inversion of image gathers would be more likely to yield AVO attributes representative of the actual angle-dependent reflectivity. In particular, we hoped that alternative robust line-fitting methods would provide a stable and more accurate characterization of AVO from the 24-fold image gathers (Figure 12). An AVO attribute that we found useful at Teal South is the fluid factor (Smith and Gidlow, 1987). When calculated after prestack migration, a fluid factor anomaly (Figures 12 and 13) associated with the 4500-ft sand facilitates interpretation of the extent of the pay and its terminations updip (against the fault) and downdip (at the oil-water contact).

Conclusions. In spite of the sparse receiver grid, we obtained useful AVO attributes for the reservoir. This depended on its AVO response being sufficiently well sampled by the OBC survey, and that its response was preserved through the processing sequence. Based on our results from synthetic and real data, the wave-equation-based depth migration algorithm we applied to migrate CRGs appears to have been a useful addition to the AVO preprocessing sequence.

For the real OBC data, the model-based compensation scheme for source-grid footprint effects made less difference than anticipated after the synthetic-data tests. However, we feel it deserves more study.

The imaging procedure appears to have worked well at Teal South, where the overburden is relatively simple. Elsewhere, complex overburden could lead to significant spatial variations in target illumination. In such cases, compensation for variable illumination will be necessary, perhaps by modifying the migration imaging condition. We would also expect to need a more versatile technique for calculating incidence angles.

Suggested reading. "Vertical cable as a subsalt imaging tool" by Krail (*TLE*, 1994). "4C/4D at Teal South" by Ebrom et al. (*TLE*, 1998). "Weighted stacking for rock property estimation and detection of gas" by Smith and Gidlow (*Geophysical Prospecting*, 1987). TLE

Acknowledgments: The authors thank ChevronTexaco Exploration and Production Technology Company for permission to publish this work.

Corresponding author: guypurnell@chevrontexaco.com